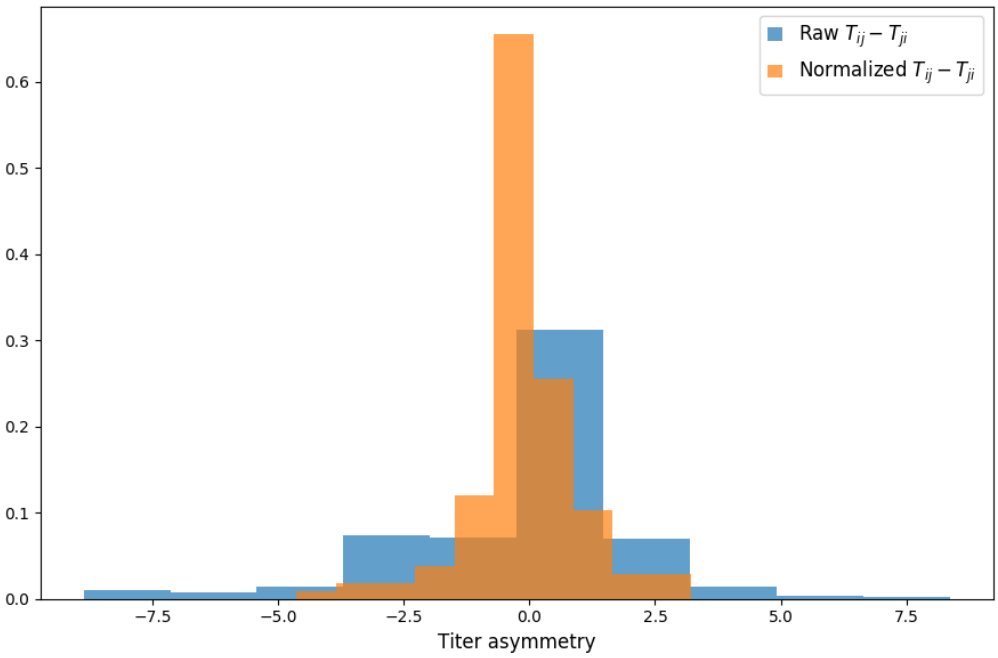

Figure 1–Figure supplement 1. Titer value symmetry. Some viruses have greater avidity overall, and some sera are more potent overall. We normalize for these row and column effects (v_a and p_b, respectively) in the titer model. Once overall virus avidity and serum potency are accounted for, titers are roughly symmetric (i.e., $D_{ij} \approx D_{ji}$).

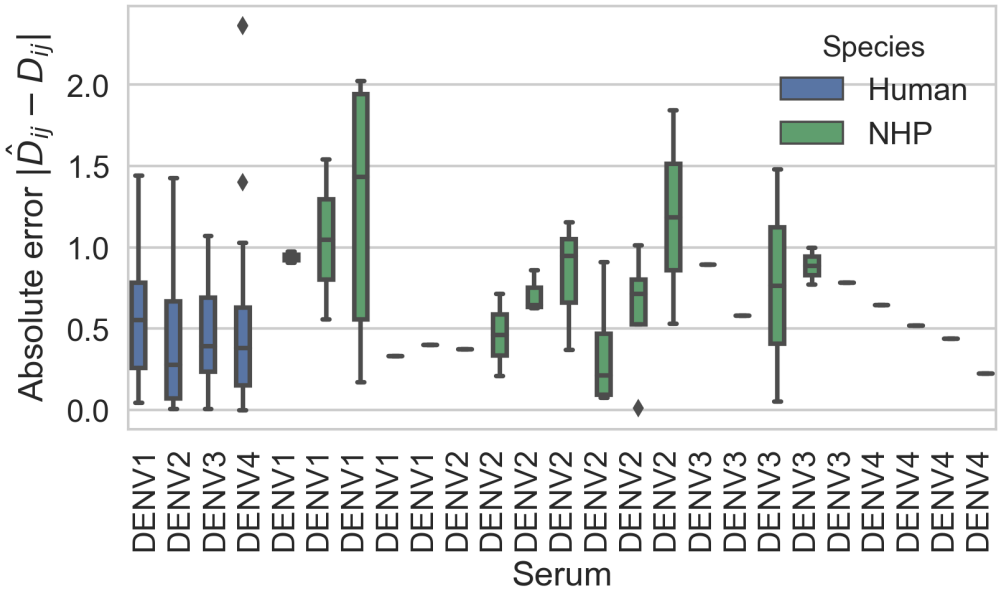

Figure 2–Figure supplement 1. Titer prediction error by serum strain and species. Human sera was raised against four different virus strains (the monovalent vaccine components); non-human primate (NHP) sera was raised against many different virus strains. Here, we excluded NHP sera raised against the monovalent vaccine components, such that each normalized titer measurement is aggregated across individuals, but not across species. We report the out-of-sample titer prediction error for each serum strain (versus all available test viruses), aggregated across 100-fold Monte Carlo cross-validation.

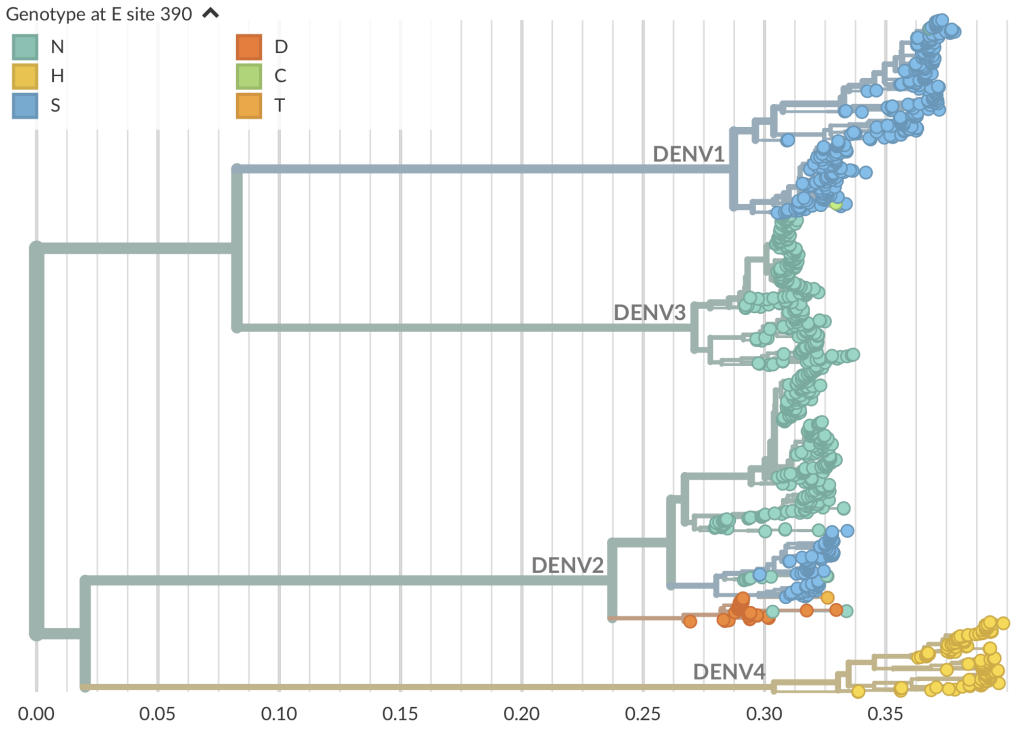

Figure 2–Figure supplement 2. Genotype as site E 390 across dengue phylogeny. Dengue virus genotypes can be seen on Nextstrain (***Hadfield et al., 2018***). A live view of this figure is available at nextstrain.org/dengue/.

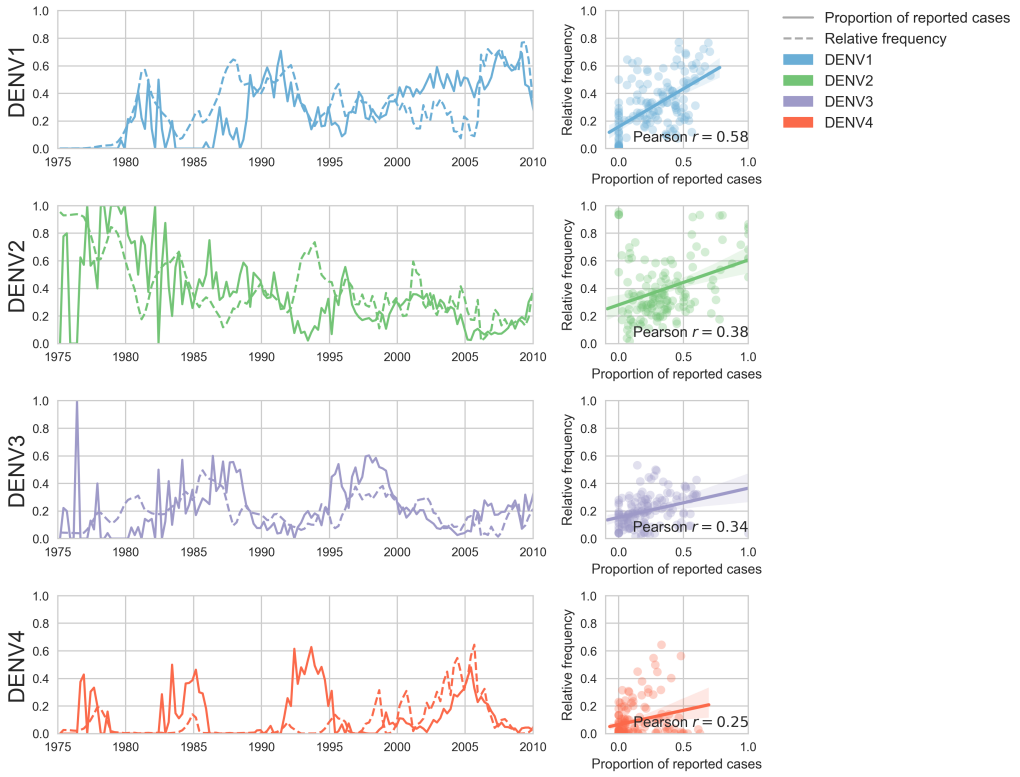

Figure 5–Figure supplement 1. Case counts versus clade frequencies in Thailand. As described in the Methods, we estimate clade frequencies based on observed relative abundance in the 'slice' of the phylogeny at each quarterly timepoint. These frequency estimates are smoothed using a discretized Brownian motion diffusion process. Here, we compare estimated serotype frequencies across Thailand (all available high quality sequences) to case counts from a hospital in Bangkok between 1975–2010 (***Reich et al., 2013***). Biweekly case counts were aggregated into quarterly timepoints, but were not smoothed. While there are some instances where case counts and frequencies diverge (e.g., DENV4 in the early 1990s), the noisy nature of the unsmoothed case counts artificially deflates estimates of concordance.

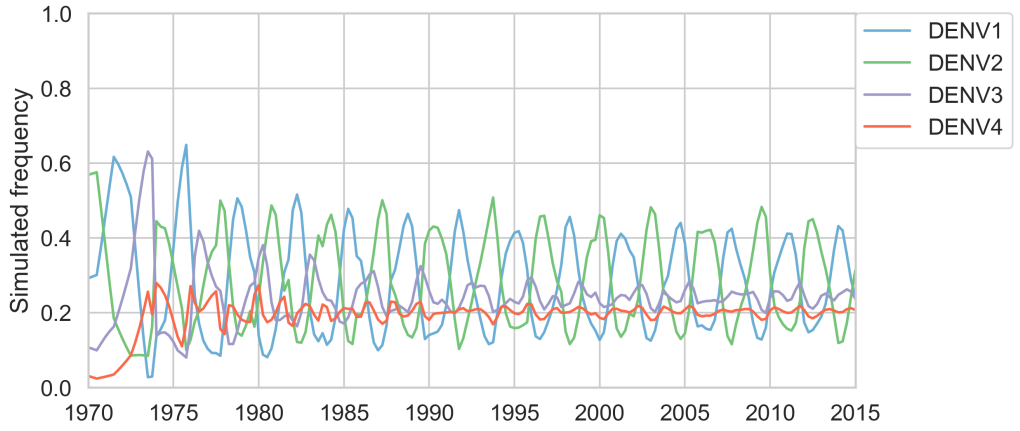

Figure 5–Figure supplement 2. Simulated serotype frequencies. As described in the Methods, we seeded a simulation with two years of empirical frequencies and predicted forward to simulate the remainder of the timecourse. Here, we simulated under the model parameters described in Table 5.

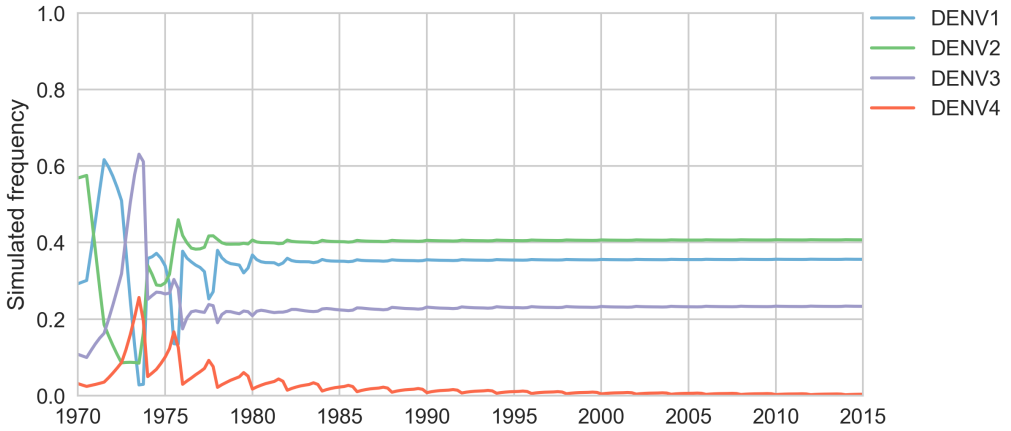

Figure 5–Figure supplement 3. Simulated serotype frequencies (model parameters). As described in the Methods, we seeded a simulation with two years of empirical frequencies and predicted forward to simulate the remainder of the timecourse. Here, we simulated under the model parameters described in Table 4. This results in damped oscillations around the intrinsic fitness value for each serotype, but these intrinsic fitnesses alone are unable to predict observed clade dynamics (Table 2).